J Mater Sci (2009) 44:2805–2813
DOI 10.1007/s10853-009-3369-z

Investigation of the thermal and structural properties of single-molecule magnet/polymer nanocomposite films

Lucas P. Johnson · Janis G. Matisons

Received: 15 October 2008 / Accepted: 23 February 2009 / Published online: 13 March 2009

Abstract The inclusion of manganese-based single-molecule magnets (SMMs) into solvent cast films of poly(methyl methacrylate) (PMMA) or polycarbonate (PC) was found to influence the thermal stability of these polymers. Examination of the thermal decomposition profiles of PMMA films by thermo-gravimetric analysis (TGA) established that increasing weight % of SMM results in both enhancement of the rate of decomposition initiated at "head-to-head" linkages along with suppression of the rate of decomposition initiated at vinylidene chain ends. In the case of PC films, the temperature at which the primary thermal decomposition occurs decreases with increasing weight % of SMM. The extent of these decomposition trends is correlated to the degree of SMM dispersal, as studied by transmission electron microscopy (TEM). Favourable interactions between the ligands coordinated to the SMMs and the polymer or solvent used in film preparation dictated the degree of SMM dispersal, with the ligand–polymer interactions being dominant on the nano-length scale (1–100 nm) and ligand–solvent interactions being dominant on the micro-length scale (>100 nm).

Introduction

Developments over the last few decades in communications and computer technology have lead to an explosion in the amount of information created worldwide. Given that it has been projected that the amount of information created will very soon exceed the capacity to store such information, it is clear that new data storage technologies must be developed to keep up with such ever increasing demand [1]. One way in which such improved data storage devices could be made is through the utilization of a relatively new class of molecules known as single-molecule magnets (SMMs). SMMs are molecular clusters that consist of either organic radicals or oxygen-bridged transition metal or rare earth atoms that are capped by a shell of organic ligands [2]. These discrete molecules are unique in that they each act as an individual magnet, as opposed to a traditional magnet, where the magnetic properties result from interactions within the bulk solid [3]. The magnetic properties of SMMs arise due to (1) the presence of a large number of spin-coupled unpaired electrons and (2) a high degree of uniaxial magnetic anisotropy [4, 5]. The spin of these electrons is coupled such that the molecule has a high overall electronic spin and therefore magnetic moment. The magnetic anisotropy means that the SMM has two preferred magnetic moment orientations; parallel and anti-parallel to the molecules "anisotropy" axis as represented by the ground states in a two well energy system (Fig. 1) [6].

Taken together, these two properties result in a significant energy barrier that must be overcome for the SMM to switch magnetic moment orientation (Fig. 1a). If the available energy is much lower than required to overcome this energy barrier (represented by the so-called blocking temperature) [7], then the SMM's magnetic moment can be magnetized in one direction by applying a magnetic field along the anisotropy axis (Fig. 1b) and will remain so for a period of time after the magnetic field is removed (Fig. 1c). This unique capacity for magnetization of individual SMMs, in addition to their small sizes (10–20 Å), makes

L. P. Johnson (✉) · J. G. Matisons
School of Chemistry, Physics and Earth Sciences, Flinders University, Sturt Rd, Bedford Park, Adelaide, Australia
e-mail: lucas.johnson@flinders.edu.au;
john0482@flinders.edu.au

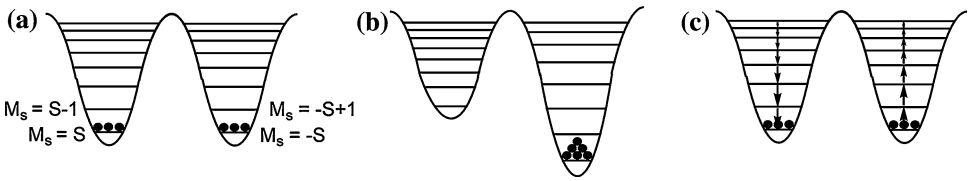

Fig. 1 Energy-level diagram for the magnetization of SMMs at low temperature **a** at thermal equilibrium, **b** when a magnetic field is applied in the direction parallel to the anisotropy axis resulting in magnetization of the SMMs, **c** when the magnetic field is removed and the SMMs slowly flip magnetic moment alignment through thermally activated and/or tunnelling mechanisms to regain thermal equilibrium [2]

these molecules ideal for use in high-density data storage devices [8].

Motivated by this potential application for SMMs, a large body of research has been produced involving the formation of films containing SMMs (both within materials and onto surfaces), a requirement if SMMs are to be addressed individually as is required in data storage devices. A number of different approaches have been explored to date including:

(1) formation of Langmuir–Blodgett films using hydrophobic or hydrophilic ligands [6, 9–12];
(2) immobilizing SMMs in sol–gel matrices [13];
(3) grafting onto gold surfaces [14–21];
(4) grafting onto Si/silica surfaces [22–25];
(5) forming frozen glasses that contain SMMs [26];
(6) forming polymer films containing SMMs [27–30].

For the most part, such research has focused upon the magnetic properties of the SMMs after inclusion into films. Only recently, research has begun to be conducted regarding the structure of these films such as the distribution of SMMs and the factors that influence these structural arrangements [18, 31–34]. Such information is important as the film structure may have an impact upon the magnetic properties of the SMMs, i.e. isolated molecules versus crystallites, and will allow for an understanding of the requirements for the controlled formation of films with SMMs arranged into addressable domains [35]. Furthermore, little to no research has been conducted regarding the influence of the SMMs upon the physical properties of such films (when SMMs are included into substrates). Any changes that the SMMs bring about to film properties are important to consider if such films are to be used in devices.

To this end, our research has investigated some of these relatively unaddressed areas. Hybrid films consisting of polymers poly(methyl methacrylate) (PMMA) or polycarbonate (PC) and the SMM ($[Mn_{12}O_{12}(CH_3COO)_{16}(H_2O)_4] \cdot CH_3COOH \cdot 2H_2O$) ($Mn_{12}$-acetate) or its derivative ($[Mn_{12}O_{12}(CH_3(CH_2)_{16}COO)_{11}(CH_3COO)_5(H_2O)_4] \cdot 2CH_3COOH$) ($Mn_{12}$-stearate) were formed, and their structure was analysed by transmission electron microscopy (TEM)/energy dispersive X-ray analysis (EDAX), while their thermal properties were analysed by thermo-gravimetric analysis (TGA). Such films are easy to form, and the polymer helps stabilize the SMMs by reducing exposure to oxygen and water [6]. The particular polymers were chosen as they possess favourable thermal and mechanical properties. This particular SMM was targeted as it is one of the most well-studied SMMs and has one of the highest blocking temperatures of any known SMM (making it a likely candidate for use in data storage devices) [36].

Experimental

SMM synthesis

Mn_{12}-acetate

This compound was prepared using an established procedure [37]. Four grams (0.0163 mol) of $Mn(CH_3COO)_2 \cdot 4H_2O$ were added to 40 mL of a 60% (v/v) solution of acetic acid and distilled water. This mixture was stirred until the $Mn(CH_3COO)_2 \cdot 4H_2O$ dissolved, upon which 1 g (0.00633 mol) of $KMnO_4$ was added over the course of 2 min with stirring. Once the $KMnO_4$ had dissolved, the solution was allowed to stand for 3 days, over which time small rectangular black crystals of Mn_{12}-acetate formed. These crystals are collected by vacuum filtration, washed with acetone and stored at low temperature. FTIR (cm^{-1} ATR): (C–H) 2933, 2990; $(OC–O)_{asym}$ 1705 (free acid), 1552 (ligand); $(OC–O)_{sym}$ 1380, 1331; (Mn–O) 710, 602.

Mn_{12}-stearate

This compound was prepared using the following literature procedure [6]. An amount of 1.1 g (0.00387 mol) of stearic acid was added to a slurry of 0.5 g (0.000243 mol) Mn_{12}-acetate in 25-mL dichloromethane, and the mixture is stirred overnight. The solvent and exchanged ligands are then removed in vacuo. The residual powder is then dissolved in diethyl ether with sonication, filtered, and the solution layered with hexane. The layered solution is left to

stand at −5 °C for several hours. The resulting precipitate, Mn_{12}-stearate, is then filtered, washed with hexane and then dried in air. FTIR (cm^{-1} ATR): (C–H) 2915, 2848; $(OC–O)_{asym}$ 1572 (ligand); $(OC–O)_{sym}$ 1466, 1415, 1316; (Mn–O) 719, 606.

Film formation

Polymer films containing the above synthesized SMMs were formed using a solvent casting method. In a typical preparation, 80 mg of polymer (PC or PMMA) is dissolved in 8-mL chloroform (99.7% purity). Separately, the desired mass of SMMs (Mn_{12}-acetate or Mn_{12}-stearate) is dissolved in chloroform [or acetonitrile (99.7% purity)], and the SMM solution is added to the polymer solution. The polymer/SMM solution is then cast into a Teflon dish and the solvent evaporated at 85 °C overnight to yield smooth light brown films. As Mn_{12}-acetate is only sparingly soluble in chloroform, the Mn_{12}-acetate is initially dissolved, the solution decanted, and the remaining solid dried and weighed, in order to determine the mass of SMM that did dissolve. Mn_{12}-stearate is soluble in chloroform owing to its extended non-polar ligands.

TEM samples

Films for TEM analysis (<100 nm thick) were prepared in a similar manner to the thicker sample films, except that instead of casting the solution, a clean glass slide is dipped into the solution and dried at room temperature under an overturned watch glass to protect the film from dust.

Electron microscopy

TEM was performed using a Philips CM 100 Transmission Electron Microscope operated at 80 kV or a Philips CM 200 Transmission Electron Microscope operated at 200 kV, both with a resolution of 1 nm. Samples are prepared for microscopy by removing polymer/SMM films prepared on glass slides by cutting with a razor blade and floating off onto water. The film is then mounted onto a copper TEM grid (200 lines per inch mesh) and allowed to dry in air, before being carbon coated. Energy dispersive X-ray analysis was performed using the CM 200 instrument with an attached Ametec EDAX Genesis X-ray detector. This provided elemental analysis of features observed in the images in order to confirm these were SMMs.

Thermo-gravimetric analysis

TGA was performed using a TA instruments Hi-Res modulated TGA 2950HR instrument. All samples were heated from room temperature to 950 °C at a rate of 10 °C/min under a nitrogen atmosphere with a flow rate of 50 mL/min. Samples are dissolved in the pans using chloroform and the solvent removed by gentle heating in the same manner as for previous film formation. In this way, the samples were prevented from being blown off the pans due to the nitrogen gas flow through the furnace.

Results and discussion

Electron microscopy

A number of samples were prepared for analysis by TEM to study the influence of polymer, ligand, and solvent choice upon the hybrid film structure. Comparison with TEM images of pure polymer films and elemental analysis by EDAX confirmed that all observed features are due to the inclusion of SMMs into the films (dark objects due to their greater electron density compared to the polymer). Previous work has shown that the SMMs remain intact when processed in such solutions [2].

Figure 2 shows TEM images of Mn_{12}-acetate/PMMA hybrid film prepared using chloroform to dissolve the polymer and either chloroform or acetonitrile to dissolve the SMMs in order to study the influence of solvent choice upon film structure.

The most notable features of these images are the presence of large inhomogeneously distributed aggregates of Mn_{12}-acetate on the micrometre scale when chloroform is exclusively used in film preparation, the absence of aggregates on the same length scale when acetonitrile is used to dissolve the SMMs, and the presence of small (several nanometre) homogeneously distributed SMM aggregates on the nanometre scale regardless of the solvents used. These results suggest that, as expected, use of a solvent that is more compatible with the SMM's ligands (acetonitrile is more polar than chloroform and so is more compatible with the SMM's acetate ligands) will result in a high level of dispersion and hence, no large aggregates. However, the same film structure exists on the nanometre scale regardless of the solvent compatibility with the SMM ligands. The spherical low electron density regions for samples where acetonitrile is used are suggested to be void spaces within the polymer film. It is possible that such void spaces are formed during solvent evaporation from entrapped solvent (principally acetonitrile in which the polymer is immiscible) that remain after the majority of the more volatile chloroform evaporates, leaving the acetonitrile trapped within the rapidly solidifying polymer matrix. Continued heating results in much of the remaining acetonitrile and chloroform diffusing out of the polymer, leaving the observed void spaces. Acetonitrile, rather than

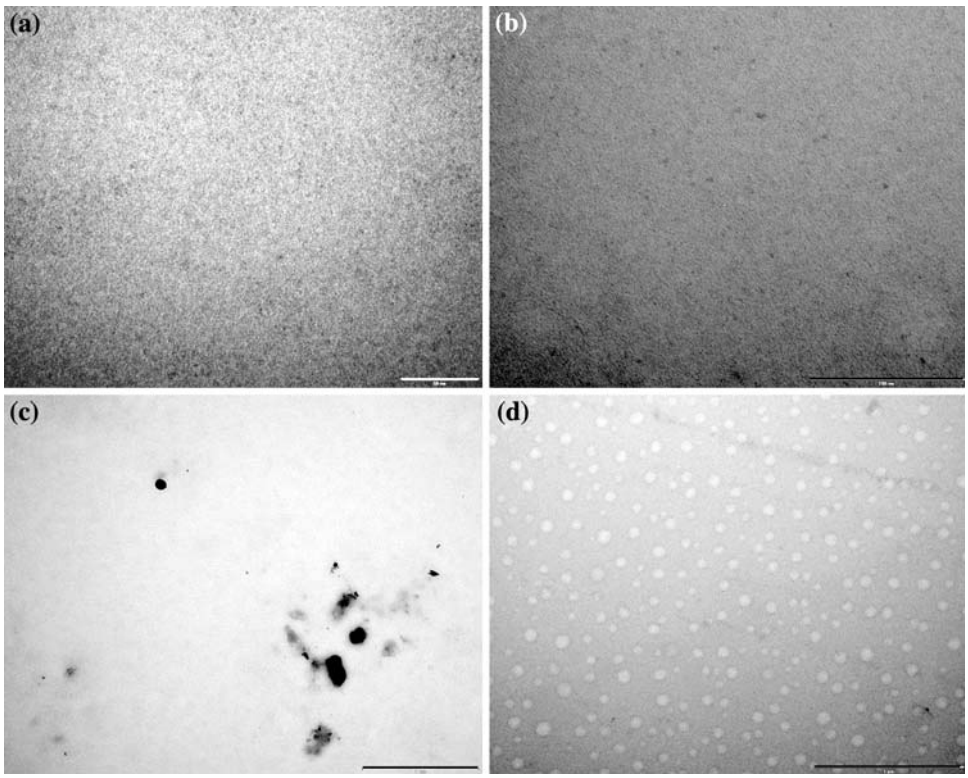

Fig. 2 TEM images of Mn_{12}-acetate/PMMA **a** prepared using chloroform, 100 nm scale bar; (**b**) prepared using chloroform/acetonitrile, 50 nm scale bar; (**c**) prepared using chloroform, 1 μm scale bar; (**d**) prepared using chloroform/acetonitrile, 1 μm scale bar

any polymer immiscible impurities, is the most likely candidate, principally due to the vast number of such void spaces observed within the polymer and the high purity of the acetonitrile (99.7%). Interestingly, despite this SMM being highly soluble in acetonitrile, the SMM clusters on the nanometre scale do not appear to be concentrated in or immediately around these voids (Fig. 3). This, together with the lack of difference between the film structures on the nanometre scale when different solvents are used, suggests that some factor other than the solvent used is dominant in determining the film structure on the nanometre scale.

Figure 4 shows TEM images of polymer films prepared using chloroform and different combinations of PMMA and PC with Mn_{12}-acetate or Mn_{12}-stearate, in order to study the effect of different polymer/ligand interactions upon the film structure.

From these images, it is observed that on the nanometre scale, small SMM clusters occur in samples of Mn_{12}-acetate in PMMA and Mn_{12}-stearate in PC. However, in samples comprising of Mn_{12}-acetate in PC and Mn_{12}-stearate in PMMA, small "domains" of SMMs form, as opposed to dense clusters. As before, this can be explained through a consideration of the compatibility between the SMM ligands and the polymer the SMMs are embedded in. Polycarbonate is a more polar polymer than PMMA, as quantified by the Hildebrand solubility parameter δ, where higher values of δ indicate greater polarity. PC has a $\delta = 10.6$ while PMMA has a $\delta = 9.3$ [38]. Likewise, acetate ligands tend to be more polar than the longer chain stearate ligands, leading to greater chemical compatibility between the relatively non-polar PMMA/stearate functional SMMs. Similarly, the relatively polar PC/acetate functional SMMs (which exhibit SMM domains) also have improved compatibility. The relatively incompatible PMMA/acetate functional SMMs and the PC/stearate functional SMMs both exhibit dense SMM clusters. The

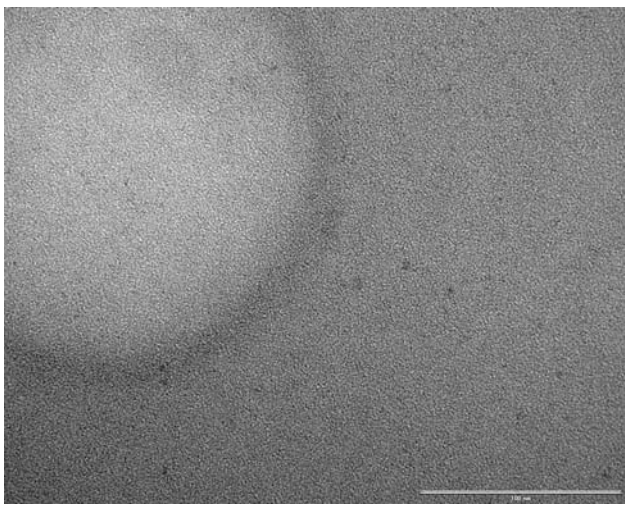

Fig. 3 TEM image of Mn_{12}-acetate/PMMA film prepared using chloroform and acetonitrile showing a void space in the polymer. Scale bar: 100 nm

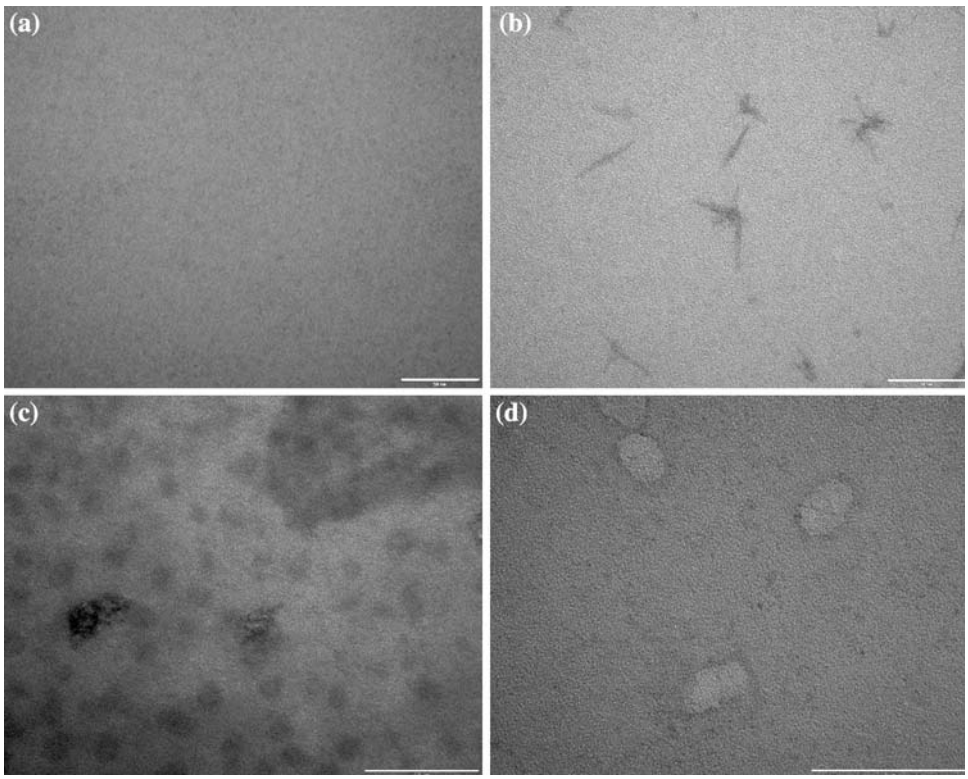

Fig. 4 TEM images of films consisting of **a** Mn_{12}-acetate in PMMA, **b** Mn_{12}-stearate in PMMA, **c** Mn_{12}-acetate in PC, **d** Mn_{12}-stearate in PC. Scale bar: 50 nm

SMMs tend to form SMM-rich "domains" as opposed to dispersing more homogeneously, so clearly there exists a balance between ligand–ligand interactions and ligand–polymer interactions, with interactions between cluster ligands being a little stronger than those between the ligands and polymer. One final observation of interest is that in those nanocomposites that displayed SMM domains, Mn_{12}-acetate tended to form somewhat spherical domains whereas the Mn_{12}-stearate tended to form needle-like domains.

Thermo-gravimetric analysis

TGA was performed on polymer nanocomposites to determine if the inclusion of SMMs has any bearing upon the thermal stability of these materials. Pure polymer, along with nanocomposites consisting of weight fractions of 0.2, 0.4, 0.6, 0.8 and 1% SMM, was analysed. The data shown is of the derivative weight loss (weight %/°C), as this gives a clearer indication of changes in sample weight as a function of temperature. Note that in the TGA data for all samples there is a broad mass loss with no derivative peak that extends from room temperature up to 200 °C. This has been ascribed to loss of residual solvent from the sample preparation process. The % mass loss due to solvent is nearly the same in all samples.

PMMA/SMM nanocomposites

Figure 5 shows TGA results for the PMMA nanocomposites.

Results for pure PMMA are as expected based on literature, which suggests that thermal decomposition of radically polymerized PMMA is a three-step process [39, 40]. As the content of SMMs in the polymer nanocomposites increases, the decomposition profile changes from that of the pure polymer. The degree of decomposition at the first mass loss step (inflection at 195 °C) is observed to increase, the degree of decomposition at the second mass loss step (inflection at 295 °C) decreases and the degree of decomposition at the third mass loss step (inflection at 380 °C) remains unaffected. The same trend occurs for PMMA nanocomposites containing both types of SMMs but occurs to a greater extent in the case of the Mn_{12}-st, with the peak corresponding to the first mass loss being broader and having its inflection at a lower temperature.

The mass losses observed are unlikely to be directly due to decomposition of the SMMs, as the peaks at which the decomposition occurs do not match those of the SMMs, and the weight loss of the polymer at these decompositions is greater than the mass of SMMs in the nanocomposite [6, 41]. Additionally, the reduction of mass loss at the second peak in the TGA with increasing SMM content affirms such mass loss arises principally from changes in the decomposition of the polymer, resulting from the inclusion of the SMMs.

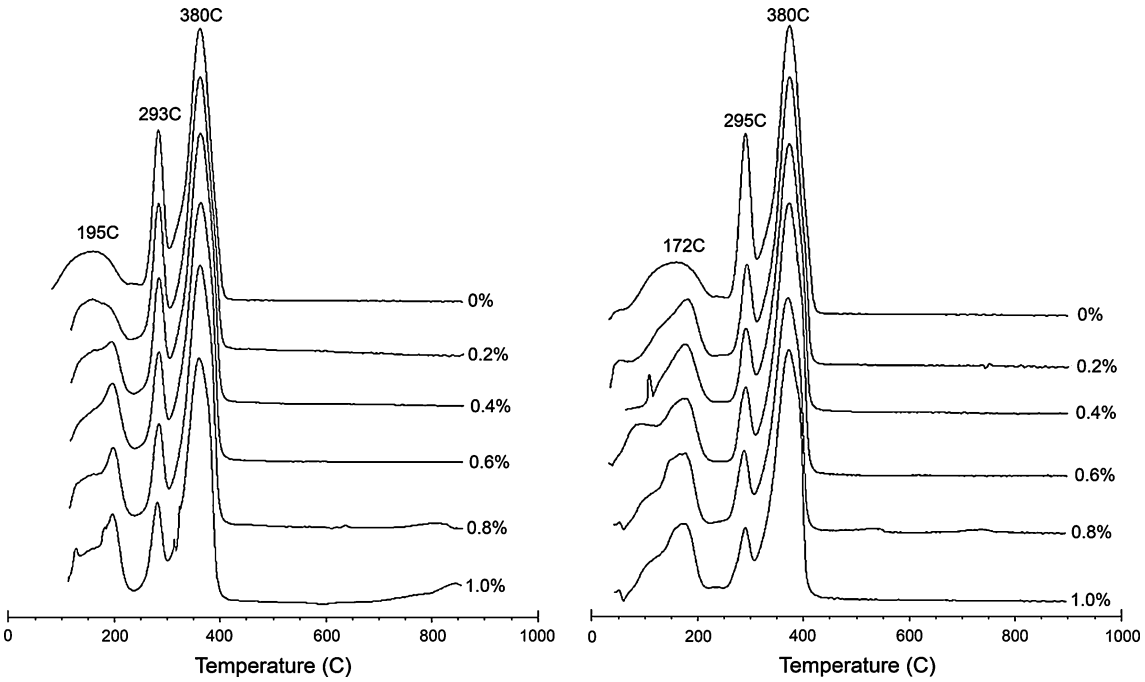

Fig. 5 *Left* TGA of PMMA Mn_{12}-ac nanocomposite. *Right* TGA for PMMA Mn_{12}-st nanocomposite. Note that polymer decomposition temperatures (195, 295 and 380 °C) derived from TGA shift from literature values (165, 270 and 360 °C) due to different heating rates and polymer molecular weight [39]

In order to understand how the SMMs influence the decomposition of PMMA, one must first consider the mechanism by which PMMA decomposition occurs (Scheme 1).

The first step of this mechanism (initiation) involves the thermally activated homolytic cleavage of a carbon–carbon bond along the polymer chain, leading to the formation of polymer radicals [39, 42]. In the case of radically polymerized PMMA, there are three possible sites along the chains at which this cleavage can occur (as depicted in Scheme 2). These are head-to-head linkages, vinylidene chain ends and normal polymer backbone linkages. Each of these linkages has different carbon–carbon bond strengths, resulting in the three distinct mass loss steps at different temperatures observed in the TGA results (head-to-head linkages being the weakest and normal backbone linkages being the strongest) [39, 40].

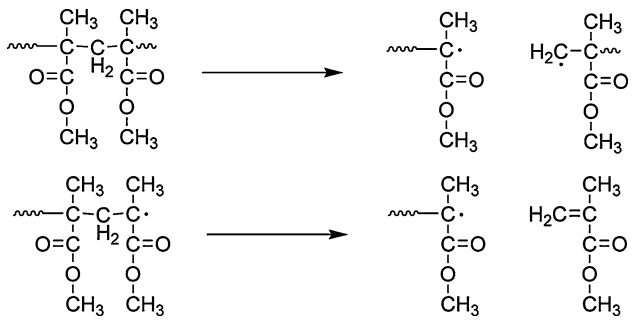

Scheme 1 Thermal decomposition mechanism of PMMA. *Top* initiation. *Bottom* β scission [39]

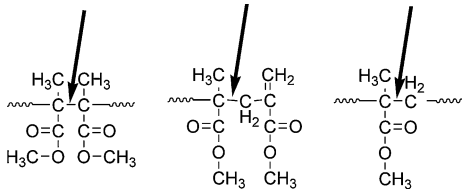

Scheme 2 Initiation sites of thermal decomposition in PMMA (indicated by an *arrow*). *Left* Head-to-head linkage. *Centre* vinylidene chain end. *Right* normal polymer backbone linkages [39, 40]

The formed polymer radicals then undergo a process known as β scission (Scheme 1), which results in the loss of a monomer unit [39, 42]. The polymer radicals continue to undergo β scission (propagation) until the radicals are terminated, whereupon β scission ceases [42]. As a result of these radical terminations, each polymer radical has a specific lifetime in which it can contribute to the decomposition of the polymer. The greater or lesser extent of mass loss at each of the decomposition steps in the TGA results for pure PMMA arises from the greater or smaller number of each linkage type within the polymer, since the same type of radical results from cleavage of each linkage type (so the radical activity is expected to be the same in each case).

The mechanism by which the SMMs influence the mass loss initiated by cleavage of head-to-head linkages is likely to be similar to that suggested by Xi et al. (in order to

explain increased thermal decomposition when metal sulphates are added to PMMA) is occurring [43]. In their work, it is explained that the activity of PMMA radicals is reduced through conjugative effects involving the ester group of the PMMA pendant chain. Cooperation occurs between the introduced metal ions associated with the sulphates and the carbonyl oxygen of the PMMA side chain ester groups (Scheme 3), resulting in a weakening of the conjugative effect of the ester group. This would then lead to the promotion of β scission, thereby resulting in an increase in the degree of mass loss before termination of the radical occurs.

Similarly, in the PMMA/SMM nanocomposites, as the content of SMMs in the nanocomposite is increased, more SMMs are available to interact with ester groups, resulting in an increase in mass loss via the mechanism outlined above. As to the greater extent of mass loss (more mass loss for a given % content of SMMs) that occurs in the case of the Mn_{12}-st/PMMA nanocomposites compared to the Mn_{12}-ac/PMMA nanocomposites, this is ascribed to the greater dispersal of the Mn_{12}-st, which would result in many more ester groups being influenced by the SMMs.

Furthermore, with regard to the peak broadening, it is possible that a similar process involving interaction of the SMMs with PMMA ester groups may weaken adjacent head-to-head linkages, resulting in homolytic cleavage of these linkages at a lower temperature than normal (note that Xi et al. also observed a reduction in the onset temperature of thermal decomposition of PMMA when metal sulphates are present) [43, 44]. This would result in two mass loss peaks due to cleavage at head-to-head linkages: one at a lower temperature due to cleavage of head-to-head linkages weakened via interaction with the SMMs and one at a higher temperature due to cleavage at head-to-head linkages that are not weakened by interaction with the SMMs. In the case of the Mn_{12}-acetate/PMMA nanocomposites, the difference in temperature of these two peaks appears to be small (indicated by a shift in the inflection point of the mass loss peak from 202 °C for pure PMMA to 195 °C for Mn_{12}-ac/PMMA), meaning that the peaks cannot be resolved (leading to a single broader peak). If this is correct, then this also suggests that Mn_{12}-ac does not weaken the head-to-head linkages to the same extent as Mn_{12}-stearate in PMMA, where the difference in temperature of these two peaks appears to be larger (inflection at 175 °C for Mn_{12}-st/PMMA), yet still not enough to resolve the peaks, resulting in a single broadened mass loss peak.

Considering the nature of this reaction mechanism, it is reasonable to presume that it would apply to decomposition (mass loss) initiated at all the different linkages in PMMA. Clearly however, this is not the case, as there is a decrease in mass loss initiated at vinylidene chain ends (with no peak broadening) and there is no change at all in mass loss initiated at regular linkages along the polymer backbone. This can be explained by considering that as the temperature increases, the SMMs themselves degrade (yielding different decomposition products). For example, Mn_{12} SMMs loose ligands at around 200 °C (between the first and second decompositions of PMMA), while the cluster core decomposes to Mn_3O_4 at around 300 °C (between the second and third decompositions of PMMA) [6, 41]. Therefore, mass loss behaviour observed at higher temperatures may well result from different derivatives of the SMMs being present. Such derivatives may not be able to form Mn–O bonds and, therefore, will not weaken the C–C bond along the backbone. Another possibility is that as the temperature increases, this intermolecular interaction weakens such that it has little or no effect upon the C–C bonds of the polymer linkages [44].

One possibility by which the intact cluster cores reduce mass loss initiated at vinylidene chain ends of PMMA is through the naked $Mn_{12}O_{12}$ clusters acting to trap the polymer-free radicals. This essentially equates to earlier termination of the polymer radicals, leading to less mass being lost per polymer radical and therefore less overall mass loss. More SMMs would increase the extent of this effect as more of the polymer radicals could then be trapped. The greater dispersal of the Mn_{12}-st complexes would also account for the greater extent of this effect in these nanocomposites. This improved thermal stability via radical trapping has been observed previously in other nanocomposites containing metal oxides and PMMA [45]. The polymer radicals formed from scission at each type of polymer linkage are essentially the same, so in our case it is not unreasonable to expect that this effect would also influence decomposition initiated at head-to-head linkages, as the SMM cluster core is intact at these lower temperatures. The fact that this mechanism does not appear to influence this mass loss may be due to the fact that the intact SMMs (with ligands) are much less accessible compared to at higher temperatures, where loss of the SMM ligands occurs. Another possibility is that radical trapping is hindered because of the interaction between the

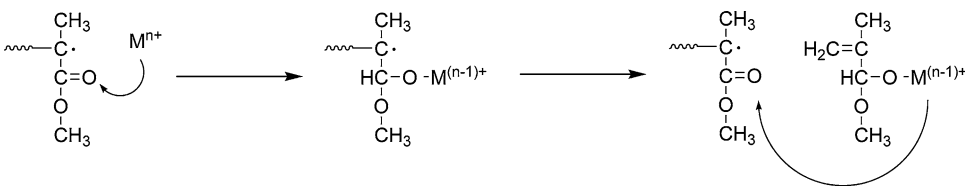

Scheme 3 The effect of metal ions on the thermal decomposition of PMMA [43]

SMM and the pendant carbonyl oxygen. The observation that decomposition initiated at regular backbone linkages is unaffected by the presence of SMMs tends to suggest that the decomposed clusters are unable to effectively trap radicals compared to the intact SMM clusters.

PC/SMM nanocomposites

Figure 6 shows TGA results for the PC nanocomposites.

The thermal decomposition profile for PC is substantially different from PMMA and, likewise, occurs through a different mechanism. From our TGA results (Fig. 6), there are two mass loss peaks: the initial peak due to loss of residual solvent and the primary decomposition peak for the PC, which is consistent with the literature [46]. When SMMs are introduced into the PC, a large decrease in the peak decomposition temperature occurs (~60 °C), with subsequent additions of SMMs further decreasing the decomposition temperature, although these are in much smaller increments (~5–7 °C). The temperature decrease is more pronounced for the Mn_{12}-ac PC nanocomposites compared to the Mn_{12}-st PC nanocomposites. It is important to note that at the decomposition temperature of PC, the SMMs would already be completely degraded to form Mn_3O_4; therefore, it is these SMM decomposition products that are responsible for the catalysed decomposition of the PC.

These results can be explained by considering similar results from a prior study by Gupta and Viswanath, where the thermal properties of composites of PC and various metal oxides were investigated [47]. They proposed that a number of metal oxides (such as MnO_2) interact with the polymer peroxide radicals that form due to thermally induced processes (such as chain scission at the carbonate bond along the polymer backbone and loss of a methyl group from the isopropylidene linkage; Fig. 7). This interaction results in the formation of peroxide–metal oxide adducts, which decompose at lower temperatures than the polymer peroxide radicals themselves and yield volatiles and unchanged metal oxide.

Greater SMM content leads to a slight reduction in the inflection point of the primary mass loss peak, as more catalyst is available to facilitate the decomposition of a greater number of radicals at any instant. This in turn leads to more mass being lost at the low temperature end of the mass loss peak for this heating rate. Mn_{12}-ac PC nanocomposites exhibit greater peak temperature decreases compared to the Mn_{12}-st PC nanocomposites, and again this is related to the improved dispersal of the SMMs. Thus, more metal oxide can interact with the radicals, leading to more radicals being decomposed at the lower temperature end of the mass loss peak.

Conclusions

Employing TGA and TEM, the thermal and structural properties of nanocomposites films of Mn_{12} SMMs with

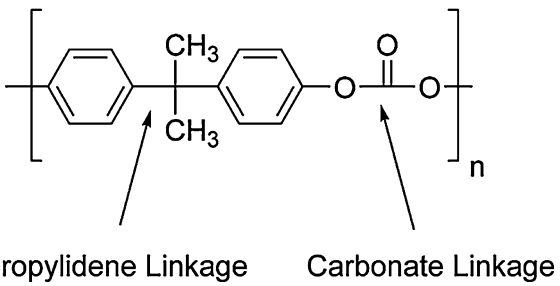

Fig. 7 Structure of bisphenol A polycarbonate

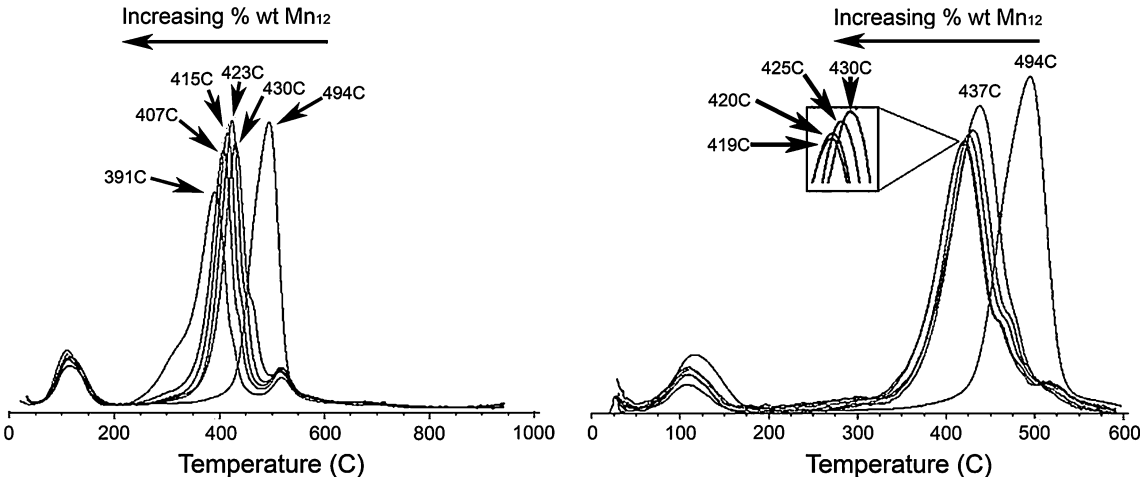

Fig. 6 *Left* TGA of PC Mn_{12}-ac nanocomposite. *Right* TGA of PC Mn_{12}-st nanocomposite

PMMA and PC were investigated. Structural studies found that compatibility between the solvent used to cast the films and the SMM ligands influenced aggregation on the microscale, but that structural features on the nanoscale remained unaffected. Conversely, compatibility between the polymer and the SMM ligands controlled the degree of aggregation on the nanoscale but did not influence the structure on the microscale. Thermal analysis showed that Mn_{12} SMMs plays a number of roles in the thermal decomposition of PMMA. At low temperatures, they act to increase the extent of decomposition, likely by weakening backbone C–C bonds through coordinating to carbonyl oxygens. As the temperature increases, the SMMs act to trap polymer radicals, thereby inhibiting decomposition. At high temperatures, the SMMs decompose such that they no longer affect the decomposition of PMMA. In the case of PC, the SMMs act to catalyse thermal decomposition, thereby lowering the temperature at which decomposition occurs.

Acknowledgement Support from Adelaide Microscopy with TEM/EDAX analysis and financial support through DEST-ISL grant (GC06005) Sol-Gel Nanotechnology: Research Applications is gratefully acknowledged.

References

1. The Expanding Digital Universe: A Forecast of Worldwide Information Growth Through 2010 (2007) http://www.emc.com/collateral/analyst-reports/expanding-digital-idc-white-paper.pdf. Accessed 15 Oct 2008
2. Gatteschi D, Sessoli R (2003) Angew Chem Int Ed 42:268
3. Berlinguette CP, Vaughn D, Canada-Vilalta C, Galan-Mascaros JR, Dunbar KR (2003) Angew Chem Int Ed 115:1561
4. Chudnovsky EM (1996) Science 274:938
5. Oshio H, Nakano M (2005) Eur J Chem 11:5178
6. Park C-D, Jung D-Y (2001) Bull Korean Chem Soc 22:611
7. Gatteschi D, Sessoli R, Cornia A (2000) Chem Commun 9:725
8. Ruiz-Molina D, Gerbier P, Rumberger E, Amabilino DB, Guzei IA, Folting K, Huffman JC, Rheingold A, Christou G, Veciana J, Hendrickson DN (2002) J Mater Chem 12:1152
9. Clemente-Leon M, Soyer H, Coronado E, Mingotaud G, Gomez-Garcia CJ, Delhaes P (1998) Angew Chem Int Ed 37:2842
10. Vaknin D, Miller LL, Eshel M, Bino A (2001) J Phys Chem B 105:8014
11. Clemente-Leon M, Coronado E, Soriano-Portillo A, Mingotaud C, Dominguez-Vera JM (2005) Adv Colloid Interface Sci 116:193
12. Coronado E, Mingotaud C (1999) Adv Mater 11:869
13. Coradin T, Larionova J, Smith AA, Rogez G, Clerac R, Guerin C, Blondin G, Winpenny REP, Sanchez C, Mallah T (2002) Adv Mater 14:896
14. Cavallini M, Gómez J, Massi M, Biscarini F, Ruiz-Molina D, Rovira C, Veciana J (2003) Trends in nanotechnology. Salamanca, Sept 2003
15. Phark S, Khim ZG, Kim BJ, Suh BJ, Yoon S, Kim J, Lim JM, Do Y (2004) Jpn J Appl Phys 43:8273
16. Cornia A, Fabretti AC, Pacchioni M, Zobbi L, Bonacchi D, Caneschi A, Gatteschi D, Biagi R, Del Pennino U, De Renzi V, Gurevich L, Van der Zant HSJ (2003) Angew Chem Int Ed 42:1645
17. Zobbi L, Mannini M, Pacchioni M, Chastanet G, Bonacchi D, Zanardi C, Biagi R, Del Pennino U, Gatteschi D, Cornia A, Sessoli R (2005) Chem Commun 17:1640
18. Mannini M, Bonacchi D, Zobbi L, Piras FM, Speets EA, Caneschi A, Cornia A, Magnani A, Jan Ravoo B, Reinhoudt DN, Sessoli R, Gatteschi D (2005) Nano Lett 5:1435
19. Phark SH, Khim ZG, Lim JM, Kim J, Yoon S (2007) J Magn Magn Mater 310:483
20. Naitabdi A, Bucher J-P, Gerbier P, Rabu P, Drillon M (2005) Adv Mater 17:1612
21. Steckel JS, Persky NS, Martinz CR, Barnes CL, Fry EA, Kulkarni J, Burgess JD, Pacheco RB, Stoll SL (2004) Nano Lett 4:399
22. Fleury B, Catala L, Huc V, David C, Zhong WZ, Jegou P, Baraton L, Palacin S, Albouy P-A, Mallah T (2005) Chem Commun 15:2020
23. Kim K, Seo DM, Means J, Meenakshi V, Teizer W, Zhao H, Dunbar KR (2004) App Phys Lett 85:3872
24. Salman Z, Chow KH, Miller RI, Morello A, Parolin TJ, Hossain MD, Keeler TA, Levy CDP, MacFarlane WA, Morris GD, Saadaoui H, Wang D, Sessoli R, Condorelli GG, Kiefl RF (2007) Nano Lett 7:1551
25. Seo DM, Meenakshi V, Teizer W, Zhao H, Dunbar KR (2006) J Magn Magn Mater 301:31
26. Domingo N, Williamson BE, Gomez-Segura J, Gerbier Ph, Ruiz-Molina D, Amabilino DB, Amabilino DB, Veciana J, Tejada J (2004) Phys Rev B 69:052405(1)
27. Palacio F, Oliete P, Schubert U, Mijatovic I, Husing N, Peterlik H (2004) J Mater Chem 14:1873
28. Ruiz-Molina D, Mas-Torrent M, Gomez J, Balana AI, Domingo N, Tejada J, Martinez MT, Rovira C, Veciana J (2003) Adv Mater 15:42
29. McInnes EJL, Pidcock E, Oganesyan VS, Cheesman MR, Powell AK, Thomson AJ (2002) J Am Chem Soc 124:9219
30. Cavallini M, Gomez-Segura J, Albonetti C, Ruiz-Molina D, Veciana J, Biscarini F (2006) J Phys Chem B 110:11607
31. Cavallini M, Biscarini F, Gomez-Segura J, Ruiz D, Veciana J (2003) Nano Lett 3:1527
32. Cavallini M, Facchini M, Albonetti C, Biscarini F (2008) Phys Chem Chem Phys 10:784
33. Cavallini M, Gomez-Segura J, Ruiz-Molina D, Massi M, Albonetti C, Rovira C, Veciana J, Biscarini F (2005) Angew Chem Int Ed 44:888
34. Martinez RV, Garcia F, Garcia R, Coronado E, Forment-Aliaga A, Romero FM, Tatay S (2007) Adv Mater 19:291
35. Akitsu T, Nishijo J (2007) J Magn Magn Mater 315:95
36. Mironov VS (2004) J Magn Magn Mater 272–276:e731
37. North JM (2004) Synthesis and characterisation of single-molecule magnets: Mn_{12}-acetate, Fe_8Br_8 and analogs. PhD thesis, Florida State University
38. Painter PC, Coleman MM (1997) Fundamentals of polymer science: an introductory text, 2nd edn. CRC Press, Florida
39. Kashiwagi T, Inaba A, Brown JE, Hatada K, Kitayama T, Masuda E (1986) Macromolecules 19:2160
40. Demir MM, Memesa M, Castignolles P, Wegner G (2006) Macromol Rapid Commun 27:763
41. Larionova J, Clerac R, Boury B, Le Bideau J, Lecren L, Willemin S (2003) J Mater Chem 13:795
42. Zeng WR, Li SF, Chow WK (2002) J Fire Sci 20:401
43. Xi GX, Song SL, Liu Q (2005) Thermochim Acta 435:64
44. Nicolais L, Carotenuto G (2005) Metal-polymer nanocomposites, 1st edn. Wiley, New Jersey
45. Wang H, Meng S, Xu P, Zhong W, Du Q (2007) Polym Eng Sci 47:302
46. Bozi J, Czegeny Z, Meszaros E, Blazso M (2007) J Anal Appl Pyrolysis 79:337
47. Gupta MC, Viswanath SG (1996) J Therm Anal 46:1671